

# 1 Micom: metagenome-scale modeling to infer metabolic 2 interactions in the microbiota.

3 Christian Diener<sup>1</sup> and Osbaldo Resendis-Antonio<sup>1,2,\*</sup>.

4 <sup>1</sup> Instituto Nacional de Medicina Genómica (INMEGEN), Mexico City 14610, México

5 <sup>2</sup> Human Systems Biology Laboratory. Coordinación de la Investigación Científica - Red de  
6 Apoyo a la Investigación, UNAM.

7 \* Corresponding author: oresendis@inmegen.gob.mx

## 8 Abstract

9 Alterations in the gut microbiota have been associated with a variety of medical conditions such  
10 as obesity, Crohn's disease and diabetes. However, establishing the causality between the  
11 microbial composition and disease remains a challenge. We introduce a strategy based on  
12 metabolic models of complete microbial gut communities in order to derive the particular  
13 metabolic consequences of the microbial composition for the diabetic gut in a balanced cohort  
14 of 186 individuals. By using a heuristic optimization approach based on L2 regularization we  
15 were able to obtain a unique set of realistic growth rates that allows growth for the majority of  
16 observed taxa in a sample. We also integrated various additional constraints such as diet and  
17 the measured abundances of microbial species to derive the resulting metabolic alterations for  
18 individual metagenomic samples. In particular, we show that growth rates vary greatly across  
19 samples and that there exists a network of bacteria implicated in health and disease that  
20 mutually influence each others growth rates. Studying individual exchange fluxes between the  
21 microbiota and the gut lumen we observed that consumption of metabolites by the microbiota  
22 follows a niche structure whereas production of short chain fatty acids by the microbiota was  
23 highly sample-specific and was altered in type 2 diabetes and restored after metformin  
24 treatment in samples from danish individuals. Additionally, we found that production of butyrate  
25 could not be easily influenced by single-target interventions.

## 26 Introduction

27           The microbial composition in the gut may be highly consequential for human metabolism  
28 and has been associated to a variety of medical conditions such as obesity, Crohn's Disease,  
29 diabetes and colorectal cancer (1–5). Nevertheless, the causality by which the microbiota may  
30 alter the host's metabolism remains unclear. Several studies have mapped microbial genes in  
31 the microbiome to particular functions (6–8), however that approach is only qualitative since the  
32 presence of a particular metabolic gene does not guarantee expression nor a change in the  
33 associated biochemical reaction. An alternative strategy to quantify the metabolic alterations  
34 that microbial community can induce in the host' metabolism is to use computational models for  
35 analyzing the fluxes in biochemical networks (9, 10). Even though direct measurement of fluxes  
36 by carbon or nitrogen labeling is costly, one can usually approximately infer the metabolic fluxes  
37 of a particular model organism using genome-scale metabolic models. For individual bacteria,  
38 metabolic modeling using flux balance analysis (FBA) has shown to be a valuable tool to  
39 explore their respective metabolic capacities and has been used extensively in basic research  
40 and biochemical strain design (11–13). In FBA, fluxes are usually approximated from a genome-  
41 scale model containing all known biochemical reactions by maximizing the production of  
42 biomass under various constraints mirroring the enzymatic, thermodynamic and environmental  
43 conditions (12). For instance, one can restrict metabolic import fluxes to the ones whose  
44 substrate is present in (11, 13, 14) the media in order to simulate a particular growth medium.  
45 Extending FBA to microbial communities can be challenging due to the necessity of modeling  
46 the metabolic exchanges between individuals and suggesting a proper objective function to  
47 mimic the growth of the entire community as well as individual bacterial species.

48           In many cases one only maximizes the overall growth rate of the entire community which  
49 may be problematic since individual species might be competitive and will rather maximize their  
50 own growth rate than the growth rate of the community. More complex methods such as  
51 OptCom thus try to find the joint multi-objective maximum of the individual and community  
52 growth rates (15). However, those multi-objective methods are limited to communities consisting  
53 of only very few members which is not realistic for microbial communities in the gut which may  
54 contain up to several hundred distinct subpopulations (16). An additional challenge is the  
55 inclusion of abundance data obtained from 16S rRNA sequencing or metagenomic shotgun  
56 experiments into the metabolic model. This is particularly important for the metabolic exchanges  
57 taking place between different species in the same community. A highly abundant species may  
58 usually import and export much higher absolute quantities than a low abundant species which

59 will affect the resulting biochemical fluxes. Nevertheless, genome-scale metabolic modeling  
60 shows a strong potential in microbial communities as it may directly quantify the metabolic  
61 potential of a particular gut microbiota in the form of the metabolic fluxes. In particular, this  
62 computational approach predicts the metabolic exchange rates between the host and the  
63 microbial community in the gut which suggests possible mechanisms associated with the  
64 wellness or disease state of the host.

65 In this work, we present a strategy that efficiently extends metabolic modeling to  
66 microbial communities. Using an iterative strategy of linear and quadratic optimizations over a  
67 community of microbial genome scale metabolic reconstructions, we were able to scale a  
68 formulation that uses the community as well as individual growth to several hundred microbial  
69 species which enables the study of realistic microbial compositions. Additionally, we explicitly  
70 included microbial abundances from metagenomic shotgun seq and realistic diets in order to  
71 make quantitative predictions regarding the metabolic consequences for the host. The entire  
72 strategy is implemented in an easy to use Python software package called “micom”. In order to  
73 assess the explicative and predictive capacities of our approach, we applied the analysis in  
74 micom to a balanced data set of 186 danish and swedish individuals distributed across healthy  
75 individuals, patients with type 1 diabetes and patients with type 2 diabetes (with and without  
76 metformin treatment). We show that individual bacterial growth rates vary greatly across  
77 samples and that a subset of bacteria often associated with health show strong  
78 interdependencies within samples. We also quantified exchanges between the gut microbiota  
79 and gut lumen and studied the effect of the microbiota composition on the production of short  
80 chain fatty acids (SCFAs) across samples from healthy and diabetic individuals with and without  
81 treatment.

## 82 Results

### 83 A regularization strategy for microbial community models.

84 Growth in microbial communities can be quantified by two classes of growth rates, the  
85 community growth rate  $\mu_c$  (in 1/h) which expresses the growth of the entire community and the  
86 individual growth rates  $\mu_i$  which measures the growth of the subpopulation  $i$  (15, 17). Here, the  
87 community growth rate  $\mu_c$  is connected to the individual growth rates  $\mu_i$  by

$$88 \quad \mu_c = \sum_i a_i \mu_i \quad (1)$$

89 where  $a_i$  denote the relative abundance for the subpopulation  $i$  (the fraction of the community  
90 that is constituted by this subpopulation). Even though FBA can be used to obtain the maximum  
91 community growth rate, one can see from equation 1 that there is an infinite combination of  
92 different individual growth rates  $\mu_i$  for any given community growth rate  $\mu_c$  (see Figure 1A for an  
93 example). Various strategies have been employed in order to deal with this limitation, the most  
94 common one being just reporting any one of the possible growth rates distributions for  $\mu_i$ . Other  
95 approaches have tried to find the set of growth rates that maximize community growth and  
96 individual growth at the same time (15), but this is computationally intensive and may not scale  
97 well to the gut microbiota which is composed by at least tens of different genera and hundreds  
98 of different species (16, 18). Thus, we tried to formulate a strategy that would allow us to  
99 identify a realistic set of individual growth rates  $\mu_i$  and which would still scale to large  
100 communities. The simplest case of a microbial community is a community composed of two  
101 identical clonal subpopulations of the same bacterial strain each being present in the same  
102 abundance (thus constituting 50% of the community each). Assuming that the maximum  
103 community and individual growth rates are equal to one there are now many alternative solutions  
104 giving maximal community growth as shown in Figure 1A. However, the two populations are  
105 identical one would expect that both grow at the same rate. In order to enforce a particular  
106 distribution of individual growth rates one can try to optimize an additional function over the  
107 individual growth rates  $\mu_i$ . This is known as regularization and the two most common strategies  
108 are L1 regularization which minimizes the sum of individual growth rates and L2 regularization  
109 which minimized the sum of squares of the growth rates (19, 20). Here, only the L2 norm  
110 correctly identifies the alternative solution where both subpopulations grow at the same rate as

111 optimal. The same strategy can be applied to heterogeneous microbial communities composed  
112 of several subpopulations with different abundances. Here the L2 norm will give the distribution  
113 of growth rates were growth is distributed as evenly as possible across the individual  
114 populations, which allows growth for as many sub-populations as possible. Thus, the L2 norm  
115 minimization can be interpreted as a heuristic for the simultaneous maximization of individual  
116 growth rates attempted in the non-convex multi-objective formulation. This is also consistent  
117 with the demand that a subpopulation observed in the gut microbiota should be able to grow in  
118 the gut. Additionally, the L2 norm has a unique minimum. Thus, there is only one configuration  
119 of individual growth rates  $\mu_i$  that minimizes the L2 norm for a given community growth rate  $\mu_c$ . In  
120 practice, maximal community growth might only be achievable if a large fraction of  
121 subpopulations are excluded from growth, for instance by giving all resources to a fast growing  
122 subpopulation. Again, this would be inconsistent if one has prior knowledge that the other  
123 subpopulations are present in the gut and should be able to grow. Instead of enforcing the  
124 maximal community growth rate one can limit community growth to only a fraction of its maximal  
125 rate thus creating a tradeoff between fastest community growth and individual growth rate  
126 maximization. Because the community growth maximization requires full cooperativity whereas  
127 the L2 norm minimization represents egoistic individual growth maximization, we call the two  
128 step strategy to fix the community growth rate a fraction of its optimum followed by minimization  
129 of the L2 norm of individual growth rates “cooperative trade-off”.

130 Regularization by cooperative trade-off yields realistic growth rate  
131 estimates.

132 In order to test whether cooperative tradeoff yields realistic growth rates, we implemented and  
133 applied it to a set of 186 samples from swedish and danish individuals consisting of healthy  
134 individuals, individuals with type 1 diabetes and individuals with type 2 diabetes (21). Relative  
135 abundances for a total of 367 bacterial genera and 727 species were obtained with SLIMM (22)  
136 from previously published metagenomic reads (21, 22) as described in the Methods section.  
137 Abundance profiles for all identified genera across all samples were connected with the AGORA  
138 models, a set of previously published manually curated metabolic models for 773 bacterial  
139 species (23). Even though those reconstructions only accounted for 109 genera they still  
140 represented more than 99% of the total abundance of the metagenomic reads with an assigned  
141 genus (85.3% vs 85.7%, see Table 1) and in average 85% of all reads contained in each

142 sample. Even though the cooperative tradeoff strategy is applicable to species-level  
143 subpopulations, the AGORA reconstructions accounted in average only for 63% of the total  
144 reads in each sample and for less than 50% of the total reads in some samples meaning that  
145 the AGORA models would not be representative for the microbial diversity in those samples.  
146 Thus, we rather modeled the subpopulations at the genus level since this covers a larger  
147 fraction of the observed microbiota. For that individual species models from AGORA were  
148 pooled into genus-level models (see Methods). The resulting communities contained between  
149 22 and 78 genera, each represented by a full genome-scale metabolic model and connected by  
150 exchange reactions with the gut lumen. We used the relative read abundances as a proxy for  
151 the abundance of each genus in each sample. Even though DNA quantity is not an exact  
152 representation of bacterial mass (in grams dry weight) the discrepancy between the two is  
153 probably much smaller than the variation in abundances which spans several orders of  
154 magnitude (16). Import fluxes for external metabolites were restricted by applying an average  
155 western diet to each community model (23).

<b>taxa</b>	<b>unique taxa</b>	<b>assigned reads</b>	<b>with model</b>
<b>superkindom</b>	2	99.2% ± 1.5%	99.2% ± 1.5%
<b>phylum</b>	23	98.7% ± 1.5%	98.7% ± 1.5%
<b>class</b>	39	96.6% ± 1.9%	96.6% ± 1.9%
<b>family</b>	160	87.2% ± 3.8%	87.0% ± 3.9%
<b>genus</b>	367	85.7% ± 4.4%	85.3% ± 4.6%
<b>species</b>	727	68.3% ± 7.9%	63.6% ± 7.8%

156 Table 1: Distribution of taxa assignments across ranks. Shown are the number of unique taxa for each  
157 rank together with the percentage of mapped reads that could be uniquely assigned to a taxa in the rank,  
158 as well as the percentage of reads whose taxa had at least one representative in the AGORA genome-  
159 scale metabolic models. Percentages are shown as mean ± standard deviation across the 186 samples.

160 We found that computing time generally scaled well with the community size when using interior  
161 point methods which are known to provide better performance for larger models, with most  
162 individual optimizations taking less than a minute (24). However, we found that it was difficult to  
163 maintain numerical stability with large community models, thus the largest difficulty we  
164 encountered was numerical stability and not computation time. None of the tested solvers were  
165 able to converge to optimality when solving the quadratic programming problem posed by the  
166 L2 norm minimization (see Methods). Thus, we used a crossover strategy to identify an optimal

167 solution to the L2 minimization (see Methods).

168 For each of the of the 186 individual community models we solved several linear programming  
169 problems in order to evaluate the effectiveness of different optimization strategies. First, to  
170 establish a baseline we only maximized the community growth rate and used the arbitrary  
171 distribution of growth rates that is returned by the solver when applying no regularization. This  
172 was followed by applying the cooperative trade-off strategy with varying levels of suboptimality  
173 ranging from 10% to 100% of the maximum community growth rate. As argued before we  
174 observed that just optimizing the community growth rate with no regularization of the individual  
175 growth rates led to solutions where only a few subpopulations were left to grow with  
176 unreasonable high growth rates (doubling times smaller 5 minutes) whereas the rest of the  
177 microbial community did not grow (compare figures 1B-C with strategy marked by “none”).  
178 Adding the L2 norm minimization even while maintaining maximum community growth notably  
179 increased the growing fraction of the community and gave smaller growth rates overall.  
180 However, we also found that maximization of the community growth rate is generally  
181 incompatible with the assumption that the majority of the observed genera should be able to  
182 grow. Lowering the community growth rate to suboptimal levels strongly increased the growing  
183 fraction of the population where a community growth rate of 20% of its maximum will allow  
184 essentially all bacterial subpopulations to grow. Based on reports that about 20-40% of the  
185 bacteria found in stool are not viable (25), we chose a suboptimal community growth rate of  
186 50% maximum growth (which allowed growth for about 70% of all subpopulations) as the trade-  
187 off parameter for all subsequent analyses.

188 Growth rates are heterogeneous and depend on the community  
189 composition

190 The community and individual growth rates obtained this way were in good agreement with  
191 previous evidence. Bacterial communities showed an average doubling time of about 10 hours  
192 where individual genera had an average doubling time of 20 hours with a minimum of 23  
193 minutes which is consistent with the generally low growth in the gut and the fast doubling time of  
194 about 20 minutes that can be observed in laboratory growth media (26).

195 Even though community growth rates varied only little across all samples (0.069 +- 0.019 1/h)  
196 we found that individual growth rates often varied across five orders of magnitude (see Figure  
197 2). Here Eubacterium was predicted to be the fastest growing genus overall which is consistent  
198 with the ubiquitous presence of Eubacterium in microbiome samples (27, 28). We found that  
199 growth rates and abundances were not linearly correlated (Pearson R=0.0) but showed a  
200 moderate correlation on the log-log scale (Pearson R=0.69) which indicates that the relationship  
201 between abundance and growth rate weakly follows a Power law, Fig 3A. However, for any  
202 given abundance growth rates would still vary by up to two orders of magnitude (compare Fig.  
203 3A). Thus, the growth rate is related to abundance but can not simply be inferred from it.

204 To explain this variation in individual growth rate, we hypothesized that different genera might  
205 mutually influence each others growth rate, either by competition or by cooperation. In order to  
206 quantify the level of growth rate interdependencies we performed *in silico* knockouts for each  
207 genus in each sample and tracked the change of growth rate for all remaining genera in the  
208 sample (see Methods). Here we found that each individual genus' growth rate was impacted by  
209 another genus in at least one of the 186 samples. As could be hypothesized for a set of bacteria  
210 competing for the same resources, most interactions were competitive (red edges in Fig. 3B).  
211 However we observed a distinct subset of bacteria that were interconnected by a large amount  
212 of cooperative interactions (blue edges in Figure 3B). Strikingly, many of the bacterial genera  
213 contained in the group have been associated with gut health or disease, such as Anaerostipes,  
214 Blautia, Escherichia and Eubacterium (5, 29–33).

## 215 Differential analysis of minimal exchanges reveals the metabolic 216 consequences for the host

217 One of the major mode of interaction between the microbiota and the gut is by means of  
218 consumption from or secretion into the gut lumen. We quantified this effect by obtaining all  
219 import and export fluxes for the entire community and also each individual genus in the  
220 community. Because there are many alternative set of exchange fluxes for any set of growth  
221 rates we used the exchanges corresponding to the minimal medium, the set of exchange fluxes  
222 with smallest total import flux for the growth rates obtained by cooperative trade-off (see  
223 Methods). This is based on the assumption that the microbiota competes for resources with the  
224 gut and will thus favor the fastest import that yields the maximum growth rate.



225 Even though the minimization of total import flux favors simpler media compositions most  
226 samples showed a diverse consumption of metabolites from the gut, particularly using a wide  
227 array of different carbon and nitrogen sources (see Figure 4A). There was a large set of  
228 metabolites that were consumed across all samples but also a smaller set containing a some  
229 specific carbon sources such as Arabinogalactan and Rhamnogalacturonan derivatives and a  
230 few selected amino acids such as Alanine and Cysteine. Also all communities showed a net  
231 anaerobic growth as would be expected in the gut. In terms of genus-specific import fluxes most  
232 genera showed distinct growth niches with only minor overlap (see Fig. S1).

233 Export fluxes in general were pretty sparse which could again be expected from the  
234 minimization of import fluxes which avoids waste. However, export fluxes were in general much  
235 more sample-specific than imports. In particular we found a large set of metabolites that was  
236 only produced by a small set of samples and included short-chain fatty acids (SCFAs) which  
237 have been previously implicated in intestinal health such as butyrate, acetate, propionate and its  
238 precursors (1, 34, 35). In particular, we also observed a diminished production of acetate and  
239 acetate precursors in danish type 2 diabetic patients without metformin treatment compared to  
240 health individuals and this effect was reverted in metformin treated patients (Figure 4B).  
241 Similarly, butyrate production was completely abolished in danish type 2 diabetes patients but  
242 present in danish healthy and metformin treated individuals (Figure 4C). This is consistent with  
243 previous findings in danish and chinese populations (3, 21, 36). However, none of these effects  
244 could be observed in the Swedish samples indicating a population specific vulnerability for type  
245 2 diabetes related alterations in the gut microbiota (Figure 4C-D).

246  
247 Finally, we aimed to quantify whether particular single target interventions may change  
248 either the consumption or production of particular metabolites by the microbiota. For this we  
249 chose three swedish samples (normal, T2D metformin-, T2D metformin+ ) with the most diverse  
250 set of imports (largest set of imported metabolites). The impact of a particular intervention was  
251 then quantified by using the elasticity coefficients (37, 38), a dimensionless measure of how  
252 strongly a particular parameter affects a particular flux (see Methods). The specific single target  
253 interventions we tested were either increasing the availability of any single metabolite in the diet  
254 or increasing a single bacterial abundance in the community. In general we observed that  
255 samples from healthy individuals showed lower elasticity coefficients than the two type 2  
256 diabetes samples which can be interpreted as a robustness to changes (see Figure 5). Most  
257 interventions had a strong impact on the import fluxes (consumption of metabolites, yellow dots

258 in Figure 5) but not on the export fluxes (production of metabolites, brown dots in Figure 5). In  
259 particular there was no single intervention that would increase butyrate production in any of the  
260 three samples tested.

## 261 Methods

### 262 Data availability and reproducibility

263 All data to reproduce the manuscript, intermediate results as well as Python scripts to reproduce  
264 the figures in this manuscript are available at [https://github.com/resendislab/micom\\_study](https://github.com/resendislab/micom_study).  
265 Metagenomic reads for the 186 individuals were obtained from the study of Pedersen et. al. and  
266 can be downloaded from the Sequence Read Archive (<https://www.ncbi.nlm.nih.gov/sra>) with  
267 the SRA toolkit (<https://www.ncbi.nlm.nih.gov/sra/docs/toolkitsoft/>). A full list of run accession IDs  
268 for the individual samples is provided in Supplementary Data S1. All algorithms and methods  
269 used here were implemented in a Python package called “micom” and can be easily applied to  
270 different data sets. The Python package “micom” (**m**icrobial **c**ommunities) along with  
271 documentation and installation instructions is available at <https://github.com/resendislab/micom>.  
272 Micom is based on the popular COBRAPy package for the constraint-based modeling of  
273 biological networks and is compatible with its API (39). The AGORA reference reconstructions  
274 with an already applied average Western diet can be downloaded from  
275 <https://vmh.uni.lu/#downloadview>. Several methods used in micom require a an interior point  
276 solver with capabilities for quadratic programming problems (QPs) for which there is currently  
277 only commercial software available. Micom supports CPLEX (<https://cplex.org>) and Gurobi  
278 (<https://gurobi.org>) both of which have free licenses for academic use.

### 279 Metagenomic shotgun analyses

280 All metagenomic analyses were performed in R using an in-house pipeline which is available as  
281 Open Source software at <https://github.com/resendislab/microbiome>. Sample FASTQ files were  
282 downloaded using the SRA toolkit and and trimmed and filtered using the DADA2 filter\_and\_trim  
283 function (40) with a left trimming of 10 bp, no right trimming, a quality cutoff of 10 and a  
284 maximum number of 2 expected errors under the Illumina model. Abundances across different  
285 taxa levels were then obtained using SLIMM (22) which was chosen since it supported one of

286 the largest references (almost 5,000 reference bacterial genomes). In brief, all sample FASTQ  
287 files were first aligned to the SLIMM reference using Bowtie2 saving the 60 best matches for  
288 each read. Taxa abundance profiles were then obtained using SLIMM with the default  
289 parameters and assembled into a single abundance file. Genus-level quantifications for each  
290 sample were then matched to the AGORA models by their respective NCBI taxa id.

## 291 Strategies used in micom

292 Flux balance analysis obtains approximate fluxes for a given organism by assuming a steady  
293 state for all fluxes in the biological system and optimizing an organism-specific biomass  
294 reaction. Using the stoichiometric matrix  $S$  which contains reaction in its columns and  
295 metabolites in its rows this can be formulated as a constrained linear programming problem for  
296 the fluxes  $v_i$  (in mmol/[gDW h]):

$$\begin{aligned} & \text{maximize } v_{bm} \\ & \text{s. t. } Sv = 0 \\ & lb_i \geq v_i \geq ub_i \end{aligned}$$

297 The biomass reaction  $v_{bm}$  is usually normalized such that it will produce 1g of biomass which  
298 results in a unit 1/h corresponding to the growth rate  $\mu$  of the organism. The upper and lower  
299 bounds ( $lb_i$  and  $ub_i$ , respectively) impose additional thermodynamic constraints on the fluxes or  
300 restrict exchanges with the environment (in the case of exchange fluxes). In order to describe a  
301 community model containing several organisms each with a particular abundance  $a_i$  (in gDW)  
302 one usually embeds each organism in a an external compartment which represents the  
303 community environment (for instance the gut lumen for models of the gut microbiota). Adding  
304 exchanges for the environment compartment and exchanges between a particular organism and  
305 the environment one obtains a community model with the following constraints:

$$\begin{aligned} \mu_c &= \sum_i a_i \cdot \mu_i \\ \text{s. t. } \forall i: Sv &= 0 \\ \mu_i &= v_i^{bm} \geq \mu_i^{min} \\ lb_i &\geq v_i \geq ub_i \\ lb_i^{ex} &\geq a_i \cdot v_i^{ex} \geq ub_i^{ex} \\ lb_i^m &\geq v_i^m \geq ub_i^m \end{aligned}$$

306 Here,  $a_i$  denotes the relative abundance of genus  $i$ ,  $\mu_i$  its growth rate,  $v_i^{bm}$  its biomass flux,  $\mu_i^{\min}$  a  
307 user specified minimum growth rate,  $v_i^{ex}$  the exchange fluxes with the external environment, and  
308  $lb$  and  $ub$  the respective lower and upper bounds. Additionally,  $\mu_c$  denotes the community growth  
309 rate and  $v_i^m$  the exchanges between the entire community and the gut lumen. The described  
310 constraints are identical to the ones employed in SteadyCom (17, 22). These constraints are  
311 applied to all optimization problems in micom and will be further called the “community  
312 constraints”.

313 Cooperative trade-off method consists of two sequential problems. First, maximize the  
314 community growth rate  $\mu_c$  to obtain  $\mu_c^{\max}$ . Using a user specified trade-off  $\alpha$  now solve the  
315 following quadratic minimization problem:

$$\text{minimize } \sum_i \mu_i^2$$

$$\text{s.t. } \mu_c \geq \alpha \cdot \mu_c^{\max}$$

and community constraints

316  
317 The knockout for a genus  $i$  was performed by setting all fluxes belonging to this genus along  
318 with its exchanges with the external environment to zero ( $lb=0$  and  $ub=0$ ). This is followed by  
319 running cooperative trade-off on the knockout model and comparing the growth rates after the  
320 knockout with the ones without the knockout.

## 321 Solvers and Numerical stabilization

322 Most genome-scale metabolic models usually do not treat more than 10,000 variables in the  
323 corresponding linear or quadratic programming problems. However, in microbial community  
324 models we usually treat 10 to 100 distinct genome-scale models which makes the  
325 corresponding problem much larger. Unfortunately, many open and commercial solvers have  
326 difficulties solving problems of that scale, so we also implemented strategies to increase the  
327 success rate of those optimizations. All linear and quadratic programming problems were solved  
328 using interior point methods as those were much faster than simplex methods for problems with  
329 more than 100,000 variables. Here, we used Cplex but also tested all methods with Gurobi.  
330 Since growth rates tend to be small we also multiplied the objectives used in cooperative

331 tradeoff (maximization of community growth rate and minimization of regularization term) with a  
332 scaling factor in order to avoid near-zero objective coefficients. A scaling factor of 1000.0  
333 seemed to work well. Nevertheless, the default interior point methods for quadratic problems in  
334 Cplex or Gurobi were usually not capable of solving the minimization of the regularization term  
335 to optimality and usually failed due to numerical instability. However, the solutions reported by  
336 the aborted optimization run were usually close to the optimum but had the tendency to violate  
337 some numerically ill-conditioned constraints. To alleviate this problem we implemented a  
338 crossover strategy where we took the solution of the numerically ill-conditioned quadratic interior  
339 point method as a candidate solution set  $\mu_i^{ca}$ . Based on that we now optimized the following  
340 linear programming problem in order to restore feasibility:

$$\text{maximize } \mu_c = \sum_i a_i \cdot \mu_i$$

$$\text{s.t. } \mu_i \leq \mu_i^{ca}$$

and community constraints

341 Linear interior point methods are usually numerically stable so this linear programming problem  
342 can usually be solved to optimality. The maximization together with the new constraints will push  
343 the individual growth rates towards the candidate solution as long as it is numerically feasible.

344 Additionally, we found that normalizing the import fluxes to the total community mass also  
345 increased numerical instability since it leads to models where flux bounds varied up to ten  
346 orders of magnitude. A more stable strategy was to apply unscaled import fluxes and rather  
347 dividing all fluxes and growth rates by the total community mass after optimization. In general,  
348 we divided the fluxes by a total community biomass of 200g as reported recently (41).

## 349 Minimal media and exchange fluxes

350 By convention micom formulates all exchange fluxes in the import direction so that all import  
351 fluxes are positive and export fluxes are negative. Based on this, the minimal medium for a  
352 community was obtained by minimizing the total import flux:

$$\text{minimize } v_{tot} = \sum_i \{v_i^m, v_i^m > 0\}$$

$$s.t. \forall i: \mu_i \geq \mu_i^{ct}$$

$$\mu_c \geq \alpha \cdot \mu_c^{max}$$

and community constraints

353 Here  $\mu_i^{ct}$  denotes the optimal genera growth rates obtained by cooperative trade-off. The  
354 community exchanges were then obtained by extracting all  $v_i^m$ , whereas genus-specific  
355 exchanges were given by all  $v_i^{ex}$  as defined earlier.

## 356 Single target intervention studies

357 We used elasticity coefficients (37, 38) to evaluate the sensitivity of exchange fluxes to changes  
358 in exchange flux bounds (ergo diet changes) or changes in genera abundance. The logarithmic  
359 formulation of elasticity coefficients is given by

$$\varepsilon_p^v = \frac{\partial \ln |v|}{\partial \ln |p|}$$

360 where  $v$  denotes the exchange flux of interest and  $p$  the changed parameter. Since the absolute  
361 value removes information about the directionality of the flux this was logged separately to  
362 maintain this information. We used a value of 0.1 as differentiation step size in log space which  
363 which corresponds to a bound or abundance increase of about 10.5% in the native scale. To  
364 enable efficient computation elasticity coefficients were grouped by parameter, cooperative  
365 trade-off run once without modification, the parameter was increased, cooperative trade-off was  
366 run again and differentiation was performed for all exchange fluxes at once.

## 367 Discussion.

368 There is a large amount of data on microbial abundances available today. This is mostly due to  
369 the cost efficiency of abundance based experiments such as 16S rRNA sequencing or shallow

370 shotgun sequencing ([Hillmann et al. 2018](#)). However, there is also a wide interest in extracting  
371 information from abundance data that goes beyond differential abundance testing ([Gilbert et al.](#)  
372 [2018](#)). Here, metabolic modeling can be a valuable tool since it integrates a wide array of data  
373 such as full genome data underlying the individual species-level metabolic models, information  
374 about diets in the form of import flux bounds and abundance data. This allows to generate  
375 mechanistic predictions concerning the metabolism of the microbial community and its  
376 exchanges with its environment. However, the increased complexity of those models brings  
377 additional problems such as the inability to identify individual growth rates and slow  
378 computations. Here, we have provided a strategy that alleviates those limitations and allows for  
379 complex analysis of the community structure and its metabolic consequences. Our  
380 regularization strategy allows for a fast identification of unique set of individual growth rates  
381 which operate in biological realistic ranges. However, this requires certain assumptions for  
382 instance that the microbiota will prefer enabling more species or genera to grow over  
383 maximizing the growth of only a few. We feel that this assumption is supported by the  
384 observation that most microbial communities are constituted by a large amount of species.  
385 Individual growth rates for bacterial genera varied greatly across samples (Fig. 2) and were only  
386 weakly dictated by the genus' abundance in the sample (Fig. 3A). It seems that the large  
387 variation of growth rates can be explained by a dependency of the growth rate on the presence  
388 of other bacteria in the sample (compare Fig. 3B). Thus, bacterial growth in the gut microbiota is  
389 not only dictated by abundance but also by the microbiota composition itself.

390 Using cooperative trade-off we were able to estimate arising co-dependencies in 186  
391 personalized community models. Cooperative effects were limited to a small set of genera that  
392 are often associated with health or disease. The microbiota composition also has a strong  
393 influence on the metabolites produced by the community and production of important  
394 compounds such as butyrate is hardly affected by interventions once established. Additionally,  
395 the predicted effects on SCFA production by the community fall in line with previous  
396 observations and suggest a potential application of community models in order to predict the  
397 metabolic impact of a particular microbiota composition in a personalized manner. We observed  
398 particular alterations in the ability to produce important short chain fatty acids such as butyrate  
399 and acetate in danish individuals with type 2 diabetes and without metformin treatment which  
400 has been suggested before (21, 42).

401 In general we observed that changes in metabolism seemed to require rather large changes in

402 the community composition. Import fluxes varied only slightly across samples and most  
403 individual genera formed distinct niches. Furthermore, small single target interventions only had  
404 a substantial impact on the consumption rates of metabolites but could not affect the production  
405 of metabolites by the community. Still, export fluxes did vary substantially across samples with  
406 different microbiota compositions. In summary, this suggests that changes in the production of  
407 metabolites by the microbiota require relatively large scale changes in the community and can  
408 not be achieved by small-scale changes such as changing a single diet component or  
409 increasing the abundance of a single bacterial genus. We feel that this kind of conclusions might  
410 have an impact in engineering the microbiota and suggest that changes affecting the entire  
411 microbiota such as fecal transplants have a potentially higher chance of increasing the  
412 production of favorable components such as SCFAs. As such we hope that the methods  
413 introduced here will help to leverage affordable microbiome data in order to design personalized  
414 intervention strategies.



## 415 Acknowledgements

416 ORA thank the financial support of an internal grant from the National Institute of Genomic  
417 Medicine (INMEGEN/México).

## 418 Author contributions

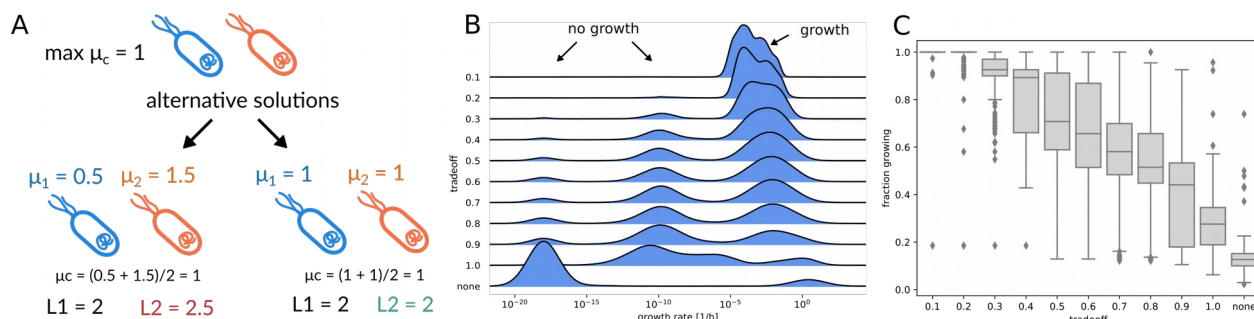
419 CD developed/implemented the methods and performed the analysis. ORA developed the  
420 methods and designed the meta-analysis. All authors wrote the manuscript.

## 421 Supplementary Material

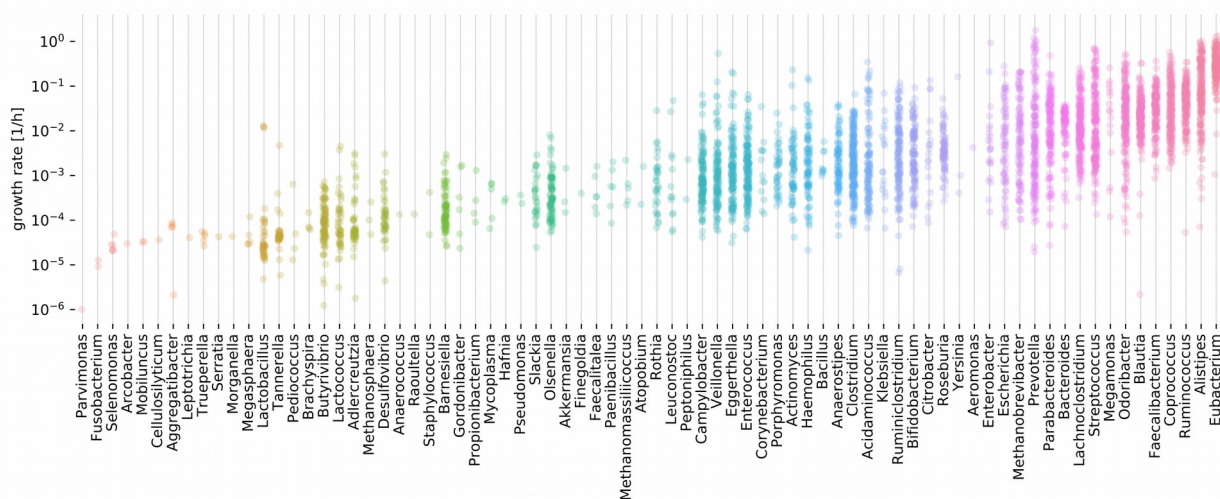
422 **Table S1.** SRA metagenome samples and metadata used to obtain microbiota compositions.

423 Additional Materials are available at [https://github.com/resendislab/micom\\_study](https://github.com/resendislab/micom_study).

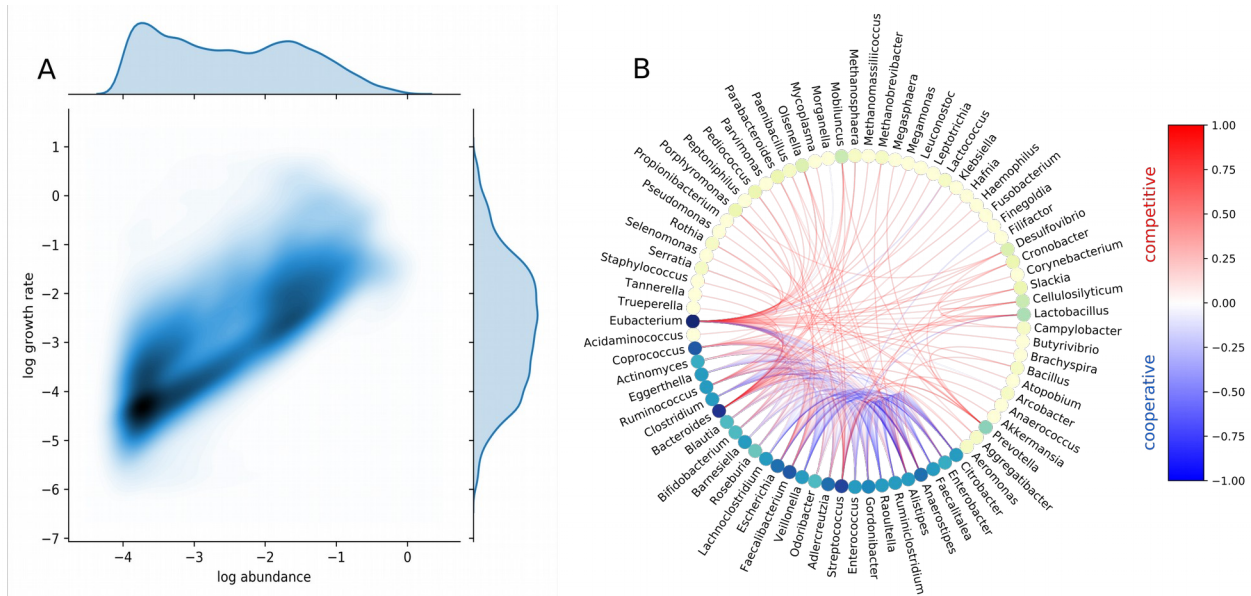
424 **Figures**



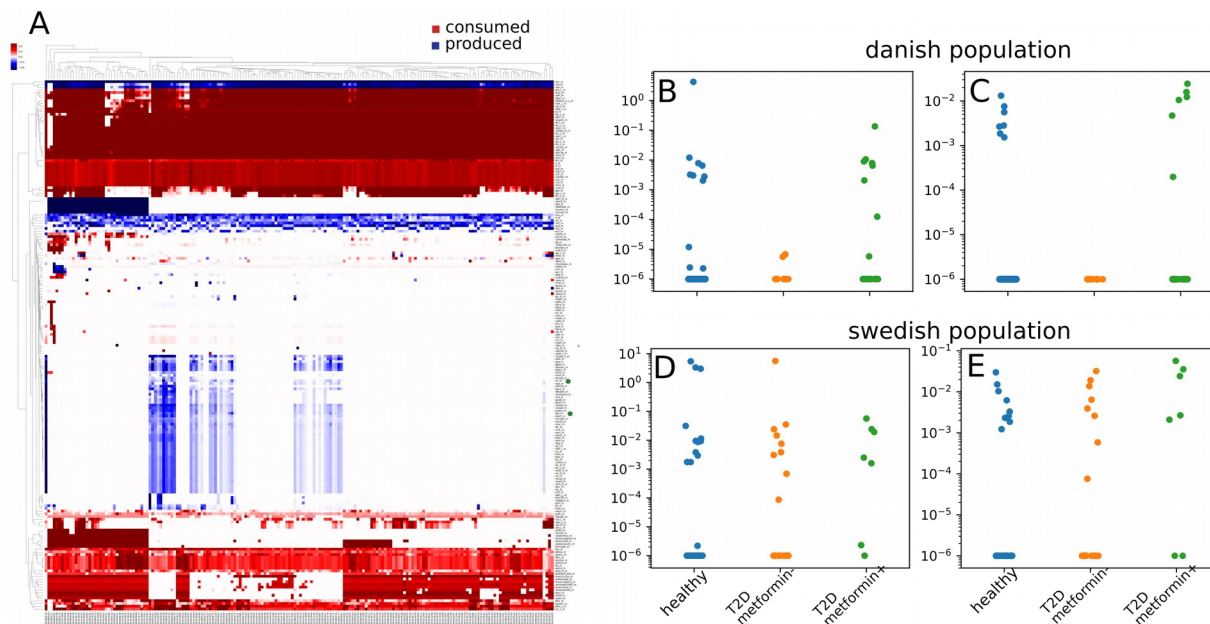
425 Figure 1: Regularization of growth rates. (A) Regularization values for a toy model of two identical *E. coli*  
 426 subpopulations. Shown are two alternative solutions with different individual growth rates and the  
 427 respective values of L1 and L2 regularization. Only L2 regularization favors one over the other and  
 428 identifies the expected solution where both subpopulations grow with the same rate. (B) Effect of different  
 429 trade-off values (fraction of maximum) on the distribution of individual genus growth rates. Zero growth  
 430 rates were assigned a value of  $10^{-16}$  which was smaller than the observed non-zero minimum. Growth  
 431 rates smaller than  $10^{-6}$  were considered to not represent growth. (C) Fraction of the overall number of  
 432 genera that were able to grow under varying trade-off values. “None” indicates a model without  
 433 regularization returning arbitrary alternative solutions.



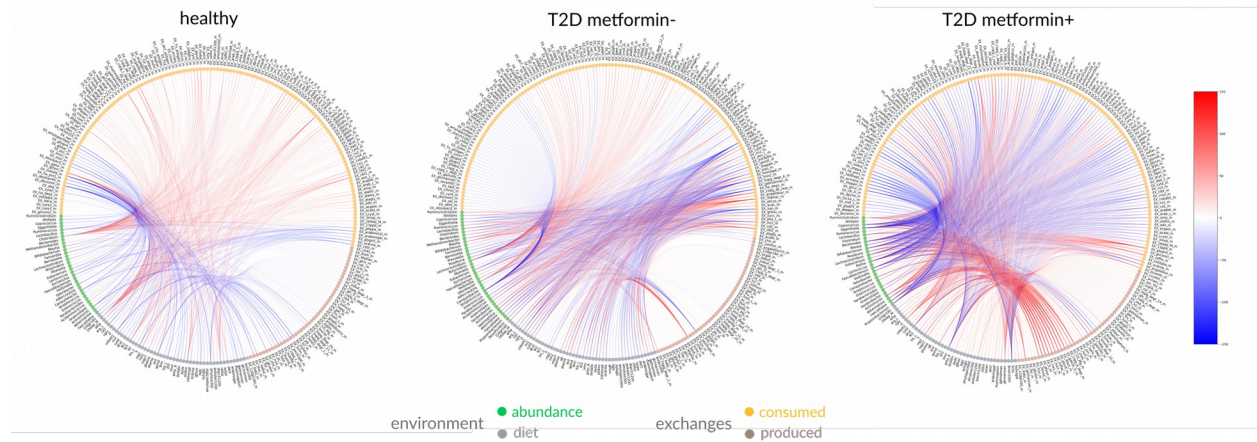
434 Figure 2: Non-zero growth rates ( $> 10^{-6}$ ) across genera obtained by cooperative trade-off (50% maximum  
 435 community growth rate). Each point denotes a growth rate in one of the 186 samples.



436 Figure 3: Co-dependencies of growth rates. (A) Genera growth rates are slightly correlated on the log-log-  
437 scale (Pearson  $R=0.69$ ,  $n=39,815$ ). Shown is the density at each point with darker blue indicating higher  
438 density. Marginal density estimations are shown on the sides. (B) Growth rate interactions between  
439 genera as estimated by genera knockouts. Shown are only interaction that induce a growth rate change  
440 of at least 50% the observed maximum. Color of edges indicates strength (in %maximum growth rate  
441 change) and type of interaction. Red edges denote competition where one removal of one genus  
442 increases the growth rate of the other and blue edges denote cooperation where the removal of one  
443 genus lowers the growth rate of the other. Nodes are colored by the degree (number of edges) from lime  
444 (low degree) to dark blue (high degree).



445 Figure 4: Exchange fluxes of the microbiota across samples. Exchange fluxes were calculated as the  
446 smallest set of import fluxes that could maintain the genera growth rates obtained by cooperative trade-  
447 off. (A) Exchange fluxes across samples. Rows were normalized to their absolute maximum and colors  
448 denote the strength and direction of exchange. Red denotes import fluxes (consumption of metabolites by  
449 the community) and blue denotes export fluxes (production of metabolites by the community). Butyrate  
450 and Acetate are marked by green dots. Acetate (B) and butyrate (C) production rates precursor in the  
451 danish population showed a drop in metformin negative T2D patients. However, in the swedish individuals  
452 this was not observed for acetate (D) nor butyrate (E).



453 Figure 5: Strong interventions across three samples. Single target interventions and their effect  
454 on exchange fluxes between the microbiota and gut lumen. Edges denote interventions and are  
455 colored by their elasticity coefficient. Shown are only interactions with an elasticity coefficient  
456 larger one (high sensitivity to changed parameter). Environmental parameters that were  
457 changed are indicated in green (microbial abundances) and gray (diet) and their exchange  
458 fluxes are colored in yellow if the microbiota produces the corresponding metabolite and in  
459 brown if the microbiota consumes the target metabolite.

## 460      **References**

- 461      1.    Cho I, Blaser MJ. 2012. The human microbiome: at the interface of health and disease. *Nat*  
462            *Rev Genet* 13:260–270.
- 463      2.    Lewis JD, Chen EZ, Baldassano RN, Otley AR, Griffiths AM, Lee D, Bittinger K, Bailey A,  
464            Friedman ES, Hoffmann C, Albenberg L, Sinha R, Compher C, Gilroy E, Nessel L, Grant A,  
465            Chehoud C, Li H, Wu GD, Bushman FD. 2015. Inflammation, Antibiotics, and Diet as  
466            Environmental Stressors of the Gut Microbiome in Pediatric Crohn’s Disease. *Cell Host*  
467            *Microbe* 18:489–500.
- 468      3.    Qin J, Li Y, Cai Z, Li S, Zhu J, Zhang F, Liang S, Zhang W, Guan Y, Shen D, Peng Y, Zhang  
469            D, Jie Z, Wu W, Qin Y, Xue W, Li J, Han L, Lu D, Wu P, Dai Y, Sun X, Li Z, Tang A, Zhong S,  
470            Li X, Chen W, Xu R, Wang M, Feng Q, Gong M, Yu J, Zhang Y, Zhang M, Hansen T,  
471            Sanchez G, Raes J, Falony G, Okuda S, Almeida M, LeChatelier E, Renault P, Pons N,  
472            Batto J-M, Zhang Z, Chen H, Yang R, Zheng W, Li S, Yang H, Wang J, Ehrlich SD, Nielsen  
473            R, Pedersen O, Kristiansen K, Wang J. 2012. A metagenome-wide association study of gut  
474            microbiota in type 2 diabetes. *Nature* 490:55–60.
- 475      4.    Livanos AE, Greiner TU, Vangay P, Pathmasiri W, Stewart D, McRitchie S, Li H, Chung J,  
476            Sohn J, Kim S, Gao Z, Barber C, Kim J, Ng S, Rogers AB, Sumner S, Zhang X-S, Cadwell  
477            K, Knights D, Alekseyenko A, Bäckhed F, Blaser MJ. 2016. Antibiotic-mediated gut  
478            microbiome perturbation accelerates development of type 1 diabetes in mice. *Nat Microbiol*  
479            1:16140.
- 480      5.    Duvallat C, Gibbons SM, Gurry T, Irizarry RA, Alm EJ. 2017. Meta-analysis of gut  
481            microbiome studies identifies disease-specific and shared responses. *Nat Commun* 8:1784.
- 482      6.    Xu Z, Malmer D, Langille MGI, Way SF, Knight R. 2014. Which is more important for

- 483           classifying microbial communities: who's there or what they can do? *ISME J* 8:2357–2359.
- 484       7. Langille MGI, Zaneveld J, Caporaso JG, McDonald D, Knights D, Reyes JA, Clemente JC,  
485       Burkepile DE, Vega Thurber RL, Knight R, Beiko RG, Huttenhower C. 2013. Predictive  
486       functional profiling of microbial communities using 16S rRNA marker gene sequences. *Nat*  
487       *Biotechnol* 31:814–821.
- 488       8. Aßhauer KP, Wemheuer B, Daniel R, Meinicke P. 2015. Tax4Fun: predicting functional  
489       profiles from metagenomic 16S rRNA data. *Bioinformatics* 31:2882–2884.
- 490       9. Bauer E, Thiele I. 2018. From Network Analysis to Functional Metabolic Modeling of the  
491       Human Gut Microbiota. *mSystems* 3.
- 492       10. Heinken A, Sahoo S, Fleming RMT, Thiele I. 2013. Systems-level characterization of a  
493       host-microbe metabolic symbiosis in the mammalian gut. *Gut Microbes* 4:28–40.
- 494       11. Resendis-Antonio O, Reed JL, Encarnación S, Collado-Vides J, Palsson BØ. 2007.  
495       Metabolic reconstruction and modeling of nitrogen fixation in *Rhizobium etli*. *PLoS Comput*  
496       *Biol* 3:1887–1895.
- 497       12. Orth JD, Thiele I, Palsson BØ. 2010. What is flux balance analysis? *Nat Biotechnol* 28:245–  
498       248.
- 499       13. Lewis NE, Hixson KK, Conrad TM, Lerman JA, Charusanti P, Polpitiya AD, Adkins JN,  
500       Schramm G, Purvine SO, Lopez-Ferrer D, Weitz KK, Eils R, König R, Smith RD, Palsson  
501       BØ. 2010. Omic data from evolved *E. coli* are consistent with computed optimal growth  
502       from genome-scale models. *Mol Syst Biol* 6:390.
- 503       14. Long MR, Ong WK, Reed JL. 2015. Computational methods in metabolic engineering for  
504       strain design. *Curr Opin Biotechnol* 34:135–141.

- 505 15. Zomorodi AR, Maranas CD. 2012. OptCom: a multi-level optimization framework for the  
506 metabolic modeling and analysis of microbial communities. *PLoS Comput Biol* 8:e1002363.
- 507 16. Thompson LR, Sanders JG, McDonald D, Amir A, Ladau J, Locey KJ, Prill RJ, Tripathi A,  
508 Gibbons SM, Ackermann G, Navas-Molina JA, Janssen S, Kopylova E, Vázquez-Baeza Y,  
509 González A, Morton JT, Mirarab S, Zech Xu Z, Jiang L, Haroon MF, Kanbar J, Zhu Q, Jin  
510 Song S, Kosciolk T, Bokulich NA, Lefler J, Brislawn CJ, Humphrey G, Owens SM,  
511 Hampton-Marcell J, Berg-Lyons D, McKenzie V, Fierer N, Fuhrman JA, Clauset A, Stevens  
512 RL, Shade A, Pollard KS, Goodwin KD, Jansson JK, Gilbert JA, Knight R, Earth Microbiome  
513 Project Consortium. 2017. A communal catalogue reveals Earth's multiscale microbial  
514 diversity. *Nature* 551:457–463.
- 515 17. Chan SHJ, Simons MN, Maranas CD. 2017. SteadyCom: Predicting microbial abundances  
516 while ensuring community stability. *PLoS Comput Biol* 13:e1005539.
- 517 18. The Human Microbiome Project Consortium. 2012. Structure, function and diversity of the  
518 healthy human microbiome. *Nature* 486:207–214.
- 519 19. Engl HW, Hanke M, Neubauer A. 2000. Regularization of Inverse Problems. Springer  
520 Science & Business Media.
- 521 20. Hoerl AE, Kennard RW. 1970. Ridge Regression: Biased Estimation for Nonorthogonal  
522 Problems. *Technometrics* 12:55–67.
- 523 21. Forslund K, Hildebrand F, Nielsen T, Falony G, Le Chatelier E, Sunagawa S, Prifti E, Vieira-  
524 Silva S, Gudmundsdottir V, Pedersen HK, Arumugam M, Kristiansen K, Voigt AY,  
525 Vestergaard H, Hercog R, Costea PI, Kultima JR, Li J, Jørgensen T, Levenez F, Dore J,  
526 MetaHIT consortium, Nielsen HB, Brunak S, Raes J, Hansen T, Wang J, Ehrlich SD, Bork P,  
527 Pedersen O. 2015. Disentangling type 2 diabetes and metformin treatment signatures in



- 528 the human gut microbiota. *Nature* 528:262–266.
- 529 22. Dadi TH, Renard BY, Wieler LH, Semmler T, Reinert K. 2017. SLIMM: species level  
530 identification of microorganisms from metagenomes. *PeerJ* 5:e3138.
- 531 23. Magnúsdóttir S, Heinken A, Kutt L, Ravcheev DA, Bauer E, Noronha A, Greenhalgh K,  
532 Jäger C, Baginska J, Wilmes P, Fleming RMT, Thiele I. 2017. Generation of genome-scale  
533 metabolic reconstructions for 773 members of the human gut microbiota. *Nat Biotechnol*  
534 35:81–89.
- 535 24. Potra FA, Wright SJ. 2000. Interior-point methods. *J Comput Appl Math* 124:281–302.
- 536 25. Maurice CF, Haiser HJ, Turnbaugh PJ. 2013. Xenobiotics shape the physiology and gene  
537 expression of the active human gut microbiome. *Cell* 152:39–50.
- 538 26. Gibson B, Wilson DJ, Feil E, Eyre-Walker A. 2018. The distribution of bacterial doubling  
539 times in the wild. *Proc Biol Sci* 285.
- 540 27. Lagier J-C, Million M, Hugon P, Armougom F, Raoult D. 2012. Human gut microbiota:  
541 repertoire and variations. *Front Cell Infect Microbiol* 2:136.
- 542 28. Koren O, Goodrich JK, Cullender TC, Spor A, Laitinen K, Bäckhed HK, Gonzalez A, Werner  
543 JJ, Angenent LT, Knight R, Bäckhed F, Isolauri E, Salminen S, Ley RE. 2012. Host  
544 remodeling of the gut microbiome and metabolic changes during pregnancy. *Cell* 150:470–  
545 480.
- 546 29. Morgan XC, Tickle TL, Sokol H, Gevers D, Devaney KL, Ward DV, Reyes JA, Shah SA,  
547 LeLeiko N, Snapper SB, Bousvaros A, Korzenik J, Sands BE, Xavier RJ, Huttenhower C.  
548 2012. Dysfunction of the intestinal microbiome in inflammatory bowel disease and  
549 treatment. *Genome Biol* 13:R79.

- 550 30. Brown K, DeCoffe D, Molcan E, Gibson DL. 2012. Diet-induced dysbiosis of the intestinal  
551 microbiota and the effects on immunity and disease. *Nutrients* 4:1095–1119.
- 552 31. Bajaj JS, Hylemon PB, Ridlon JM, Heuman DM, Daita K, White MB, Monteith P, Noble NA,  
553 Sikaroodi M, Gillevet PM. 2012. Colonic mucosal microbiome differs from stool microbiome  
554 in cirrhosis and hepatic encephalopathy and is linked to cognition and inflammation. *Am J*  
555 *Physiol Gastrointest Liver Physiol* 303:G675–85.
- 556 32. Chen W, Liu F, Ling Z, Tong X, Xiang C. 2012. Human intestinal lumen and mucosa-  
557 associated microbiota in patients with colorectal cancer. *PLoS One* 7:e39743.
- 558 33. Murri M, Leiva I, Gomez-Zumaquero JM, Tinahones FJ, Cardona F, Soriguer F, Queipo-  
559 Ortuño MI. 2013. Gut microbiota in children with type 1 diabetes differs from that in healthy  
560 children: a case-control study. *BMC Med* 11:46.
- 561 34. Kinross JM, Darzi AW, Nicholson JK. 2011. Gut microbiome-host interactions in health and  
562 disease. *Genome Med* 3:14.
- 563 35. Tan J, McKenzie C, Potamitis M, Thorburn AN, Mackay CR, Macia L. 2014. The role of  
564 short-chain fatty acids in health and disease. *Adv Immunol* 121:91–119.
- 565 36. Tremaroli V, Bäckhed F. 2012. Functional interactions between the gut microbiota and host  
566 metabolism. *Nature* 489:242–249.
- 567 37. Savageau MA. 2010. *Biochemical Systems Analysis: A Study of Function and Design in*  
568 *Molecular Biology*. CreateSpace.
- 569 38. Heinrich R, Rapoport TA. 1974. A Linear Steady-State Treatment of Enzymatic Chains.  
570 General Properties, Control and Effector Strength. *Eur J Biochem* 42:89–95.
- 571 39. Ebrahim A, Lerman JA, Palsson BO, Hyduke DR. 2013. COBRApy: COntstraints-Based

- 572 Reconstruction and Analysis for Python. *BMC Syst Biol* 7:74.
- 573 40. Callahan BJ, McMurdie PJ, Rosen MJ, Han AW, Johnson AJA, Holmes SP. 2016. DADA2:  
574 High-resolution sample inference from Illumina amplicon data. *Nat Methods* 13:581–583.
- 575 41. Sender R, Fuchs S, Milo R. 2016. Revised Estimates for the Number of Human and  
576 Bacteria Cells in the Body. *PLoS Biol* 14:e1002533.
- 577 42. Wu H, Esteve E, Tremaroli V, Khan MT, Caesar R, Mannerås-Holm L, Ståhlman M, Olsson  
578 LM, Serino M, Planas-Fèlix M, Xifra G, Mercader JM, Torrents D, Burcelin R, Ricart W,  
579 Perkins R, Fernández-Real JM, Bäckhed F. 2017. Metformin alters the gut microbiome of  
580 individuals with treatment-naive type 2 diabetes, contributing to the therapeutic effects of  
581 the drug. *Nat Med* 23:850–858.